Modeling the self-propagation reaction in heterogeneous and dense media: Application to Al/CuO thermite

Emelian Tichtchenko, Alain Estève, Carole Rossi

Modeling the self-propagation reaction in heterogeneous and dense media: application to Al/CuO thermite

Emelian Tichtchenko, Alain Estève, Carole Rossi

LAAS-CNRS, University of Toulouse, 7 Avenue du colonel Roche, 31077 Toulouse, France

KEYWORDS: Combustion, thermites, thermite, finite volume method, numerical, simulation, energetic materials, solid diffusion, flame propagation, reaction front

Abstract

This article provides a computational analysis of the reaction of fully-dense layered aluminum and copper oxide systems. After the detailed presentation of the 2D nonstationary model implementing both oxygen and aluminum diffusion, the propagation of the reaction front in an Al/CuO thin film was studied. The model qualitatively reproduces the dependency of the reaction front progression rate spatially as a function of the fuel concentration. Calculations also evidence the inverse evolution of flame front width with respect to the reaction front velocity. A procedure to estimate the heat loss generated by the fact that the reactants and products may vaporize prior to reaction completion was proposed by imposing a flame temperature limit close to Cu vaporization point. This work also shows that microscopic fluctuations in the instantaneous reaction front velocity can be observed for reactant diffusion activation energy (E_a) of 125 kJ/mol, before quenching for greater E_a. Finally, we demonstrate the potential of this new 2D nonstationary model to investigate the thermal effect of additives such as metallic impurities in the Al/CuO thin film that can lead to the flame front corrugation at the microscale. The simulations show that a metallic particle acts first to boost the reaction velocity as its high thermal conductivity helps the upfront heating. Then, the particle being also a heat sink, a local slowing down of the front velocity is observed.

Nomenclature

Symbol	Meaning	Unit
C	Total concentration of the material (equivalent to a density)	$kg.m^{-3}$
C_i	Concentration of the species *i*	$kg.m^{-3}$
C_p	Average specific heat capacity	$J.kg^{-1}.K^{-1}$
$C_{p,i}$	Specific heat capacity of the species *i*	$J.kg^{-1}.K^{-1}$
D_i	Diffusion coefficient of the species *i*	$m^2.s^{-1}$
Ea_i	Activation energy of the Arrhenius law defining the reaction rate of the copper oxide decomposition	$J.mol^{-1}$
$E_{a,CuO}^{chem}$	Activation energy of the Arrhenius law defining the reaction rate of the copper oxide decomposition	$J.mol^{-1}$
F_s	Enthalpy flux related to species flux	$kg.m^{-2}.s^{-1}$
$h_{f,i}^o$	Enthalpy of formation of the species *i*	$J.kg^{-1}$
$k_{0,CuO}^{chem}$	Pre-exponential factor of the Arrhenius law defining the reaction rate of the copper oxide decomposition	s^{-1}
$k_{0,i}$	Pre-exponential factor of the Arrhenius law defining the diffusion of the species *i*	$m^2.s^{-1}$
L	Simulated length	µm
L_t	Total thickness	µm
n	Number of bilayer	
P_{Hrx}	Power of reaction	$W.m^{-3}$
P_{PC}	Required power for phase change	$W.m^{-3}$
R	Gas constant (R=8.314)	$J.K^{-1}.mol^{-1}$
r_i	Reaction rate of the species *i*	$kg.m^{-3}.s^{-1}$
T	Temperature	K
T_{max}	Flux limiting temperature	K
t	time	s
t_{Al}	Aluminum layer thickness	nm
t_b	Bilayer thickness	nm
t_{CuO}	Copper oxide layer thickness	nm
v	Front velocity	$m.s^{-1}$
w_f	Front width	m
λ	Average heat conductivity	$W.m^{-2}.K^{-1}$
λ_i	Heat conductivity of the species *i*	$W.m^{-2}.K^{-1}$
$\varnothing_{av}$	Average heat flux going through the heat front	$W.m^{-2}$
$\varnothing_{av.loss}$	Average heat flux lost by limiting the temperature with T_{max}	$W.m^{-2}$

1 Introduction

Using nanomaterials in energetics has increased burn rates from mm/s to m/s and even km/s in some cases [1-3]. To obtain a large interfacial contact area between the fuel and oxidizer, different approaches such as ultrasonication[4], electrospraying/electrospinning mechanical milling[5-8], self-assembly (static electricity-based[9], ligand-based processes[10], sol-gel synthesis[11], DNA-based assembly[12-14], and recently 3D printing[15-18] have been explored for different applications. An alternative approach to create high density, large interface surface area composites in thermites is to fabricate nanolaminate structures through physical vapor deposition (PVD)[19-23]. Thermite nanolaminates offer a highly controllable architecture and can be incorporated into a variety of micropyrotechnic devices commonly used in microelectromechanical systems (MEMS) for tunable initiation of secondary explosives[22, 24-27], to produce safety functions[28, 29] or thrusts[30-32]. Among thermite nanolaminates, layered aluminum and copper oxide systems have drawn particular attention due to their high reactivity and gas generation ability. The effects of the different parameters of the layered Al/CuO systems with respect to bilayer thicknesses, equivalence ratios, interfacial layers (insertion of another layer between Al and CuO), and oxidation state (using Cu_2O or CuO) have been studied experimentally on the macroscopic scale[26, 33-41]. Decreasing bilayer thickness has generally a positive impact on ignition and combustion rates yielding fast reaction kinetics.

Regarding modeling, classical molecular dynamics (MD) was explored to model the reaction at the atomic scale, mostly in bimetallic systems for which good quality classical interatomic potentials are available[42, 43]. However, classical MD approaches face severe limitations in their ability to envision and describe the oxidoreduction chemical complexity of thermite materials. Some works use reactive force fields to avoid much “heavier” ab initio molecular dynamics calculations[44, 45]. Other performed DFT (Density Functional Theory)-based MD to model the onset of Al/Fe_2O_3 and Al/CuO thermites[46, 47]. While MD simulations are a valuable means of depicting atomic-scale processes, the duration of the process that can be modeled remains short, from pico- to nanoseconds, which

definitively limits their application to describe the flame front combustion dynamics over several μm thick[48]. Other attempts were proposed to extend a simple continuum approach developed for bimetallic reactive materials[49] based on the sandwich theory where overall mass transport and the reaction is assumed to follow a single Arrhenius dependence on temperature, independently of the detailed chemical composition. These attempts rapidly faced severe limitations in their ability to envision and describe the oxidoreduction chemical complexity of thermite materials. Recently, Lahiner *et al.*[50] proposed a diffusion-reaction modeling framework that considers that CuO decomposes and releases oxygen that further diffuses across the Cu_xO and Al_2O_3 layers before reacting with pure Al to form Al_2O_3. A one-dimensional oxygen mass transport equation across the layers is coupled with the one-dimensional heat equation in the flame propagation direction. Despite this crude treatment of reaction processes, the use of thermophysical properties independent of temperature and ideal layered structures, the model succeeded in demonstrating the relationship between the reaction velocity and multilayer structure. In addition, this numerical approach considering the effects of heat sinking substrate was successfully used to study the likelihood of propagating reactions[50, 51]. Precisely, the burn rate of ~4 μm thick Al/CuO nanolaminates adhered on glass substrates was no greater than 50 m/s and the reactions are less likely to quench when the substrate is thermally nonconductive (< 1.5 W/mK) which was observed experimentally. But considering a single mobile species, namely oxygen, diffusing across the various system layers, does not fit the complexity of the mechanisms occurring in thermite reactions, notably in the high temperature regime. Moreover, the 1D description of the flame propagation is a severe limitation to simulating the reaction front kinetics, for instance in treating inhomogeneities (additives, porosity), making this modeling approach unsuitable for capturing many of the existing experimental data in the field[48]. Hence, we propose a new 2D nonstationary model, based on CFD schemes and implementing more realistic reaction mechanisms that consider both oxygen and Al diffusion, since it was experimentally evidenced [52] but never explicitly introduced in thermite modelling to date. This allows the 2D temperature and species concentration distribution to

be mapped by solving the differential equations for heat and mass transport. The initial repartition and concentration of reactants can be chosen freely, hence, it is possible to simulate multilayered thermite systems (as presented herein), as well as granular reactive systems. The problem is discretized and solved using a finite volume method and coded in Python language.

In this paper, we start by detailing the general model equations. In a second stage, the model is adapted to free-standing Al/CuO multilayer systems to simulate the propagation of the reaction front in order to predict its velocity and map the temperature field. The results of varying bilayer thicknesses, equivalence ratios and film thicknesses are presented showing satisfactory agreement with the experimental tendencies presented in several preceding studies. We demonstrate that regardless of the condition of the simulation and Al/CuO configuration, the front width is inversely function of the reaction front velocity. After a parametric study of reaction velocity versus diffusion coefficients was performed, we demonstrate the potential of this new 2D nonstationary model to simulate the thermal behavior of the reaction front in the vicinity of a metallic particle embedded in the Al/CuO thin film.

2 General formulation

Two main mixing processes are supposed to drive the thermite reaction over the temperature scale. 1) At low temperatures, the statistical diffusion of mobile atoms or molecules is usually described by a Fick's law. 2) At higher temperatures, the liquid diffuses from the melted reactants through a porous media composed of reactants and products that haven't yet melted. In our approach, rather than setting the diffusion coefficient associated with the solid phases, we assume Fick's law (Equation 1) where the diffusion parameters of chemical species follow an Arrhenius dependence on temperature such that diffusion drastically increases after the melting temperature is reached.

$$\frac{\partial C_i}{\partial t} + \vec{\nabla} \cdot \left(D_i \vec{\nabla} C_i \right) = r_i \qquad (1)$$

where C_i, D_i and r_i are respectively the concentration, diffusion coefficient and rate of production of the chemical species *i*.

Then, the propagating reactions, characterized by the propagation of the thermal front, are modeled by a heat equation (Equation 2) with a source term related to the energy release during the exothermic reaction, which is written as follows:

$$\rho C_p \frac{\partial T}{\partial t} - \vec{\nabla}.\left(\lambda \vec{\nabla} T\right) + \vec{\nabla} \cdot \overrightarrow{F_s} = P_{Hrx} - P_{PC} \qquad (2)$$

where ρ, Cp, λ and P_{Hrx} are respectively the local average density, the local average heat capacity, the local average heat conductivity and the power generation due to the reaction, respectively. P_{PC} is the power required for the melting of the different species. Note that these are endothermic processes, which means that they do contribute negatively to the temperature. The vaporization of the different species is not considered in the energy as the temperature is already limited by T_{max} (further explained).

Both differential equations are coupled via the source term and energy fluxes, F_s which is related to species diffusion, as defined by Equation 3.

$$\overrightarrow{F_s} = \sum D_i \vec{\nabla} C_i \int_{298}^{T} C_{p,i}\,(T) dT \qquad (3)$$

Within each mesh the local heat capacity and heat conductivity are the average of the heat capacity and heat conductivity of each considered species weighted by their local concentration:

$$C_P(T) = \frac{\sum C_{P,i}(T)\, C_i}{\sum C_i} \tag{4}$$

$$\lambda = \frac{\sum \lambda_i\, C_i}{\sum C_i} \tag{5}$$

The heat capacity of each species is computed as a function of temperature using Shomate equation which is, for a given phase and a given species, *i*, expressed as follows:

$$C_{p,i} = A + Bt + Ct^2 + Dt^3 + \frac{E}{t^2}$$
$$t = \frac{T}{1000} \tag{6}$$

A, *B*, *C*, *D*, *E*, are known thermodynamic coefficients given in the supplementary file, Table S1.

The power of the reaction is equal to the sum of the enthalpy of formation of each species multiplied by the rate of their production, as specified in the following equation:

$$P_{Hrx} = -\sum r_i\, h^o_{f,i} \tag{7}$$

The equations are solved in the thermite system only by using a finite volume method, which is detailed in supplementary file S1. The results are the 2D temperature and species concentration mapping, from which the reaction front width (w_f) and velocity (v) are calculated as described in Sec 4.

3 Application to Al/CuO multilayered film combustion

We apply the preceding model to the simulation of the Al/CuO reaction front propagation in multilayered films composed of pure Al and CuO reactants as shown in **Figure 2**. The layers are perpendicular to the reaction propagation direction. Therefore, the species *i* are the reactants (namely Al and CuO), the products (CuO_x, Cu, Al_2O_3) and the atomic oxygen (O) upon CuO decomposition.

Despite the fact that oxygen does not appear in the main chemical reaction, it is a highly diffusive species, and has a major influence on the reaction process, notably before the melting of Al and for initiating the overall thermite reaction. Equation 1 gives the following set of equations:

$$\frac{\partial C_{Al}}{\partial t} + \vec{\nabla} \cdot \left(D_{Al}\vec{\nabla}C_{Al}\right) = r_{Al} \quad (8a)$$

$$\frac{\partial C_{CuO}}{\partial t} = r_{CuO} \quad (8b)$$

$$\frac{\partial C_{O}}{\partial t} + \vec{\nabla} \cdot \left(D_{O}\vec{\nabla}C_{O}\right) = r_{O} \quad (8c)$$

$$\frac{\partial C_{Cu}}{\partial t} + \vec{\nabla} \cdot \left(D_{Cu}\vec{\nabla}C_{Cu}\right) = r_{Cu} \quad (8d)$$

$$\frac{\partial C_{Al2O3}}{\partial t} + \vec{\nabla} \cdot \left(D_{Al2O3}\vec{\nabla}C_{Al2O3}\right) = r_{Al2O3} \quad (8e)$$

The CuO decomposition occurring prior its melting (≈700-800 K[53, 54]), the diffusion of copper oxide is considered negligible.

3.1. Chemistry and kinetic treatment

The main chemical reaction (9) can be decomposed into two subreactions (10) and (11).

$$3CuO + 2Al \rightarrow 3Cu + Al_2O_3 \quad (9)$$

$$CuO \overset{r_{CuO}}{\rightarrow} Cu + O \quad (10)$$

$$3O + 2Al \overset{r_{Al2O3}}{\rightarrow} Al_2O_3 \quad (11)$$

where r_{CuO} and r_{Al2O3} are respectively the reaction rates of reactions (10) and (11), respectively. r_{CuO} follows an Arrhenius law and is defined by Equation 12.

$$r_{CuO} = C_{CuO}^{n_{CuO}^{chem}} \times k_{0,CuO}^{chem} e^{\frac{-E_{a,CuO}^{chem}}{RT}} \quad (12)$$

The prefactor $k_{0,CuO}^{chem}$ and the activation energy $E_{a,CuO}^{chem}$ are fitted such as the decomposition of copper oxide occurring between 800 K and 1200 K[4]. n_{CuO}^{chem} is assumed to be 1. Note that in this work we consider that the CuO decomposes in one single step (CuO → Cu) as we focus on reaction front propagation dynamics occurring at high temperatures where the decomposition of CuO is not known to be a limiting process.

The reaction rate of aluminum should be considered instantaneous. Using an Arrhenius law to simulate a fast reaction would require a very small time step and drastically increase the computation time of the solver. Hence the algorithm schematized in **Figure 1** has been applied: it considers that, within a certain volume, the limiting reactant between oxygen and aluminum is completely consumed during a time step.

The model needs the material physico-thermal parameters and diffusion coefficients for each reactant. But, to determine the properties of the condensed phase reaction mechanisms one should be able to determine the characteristic time of diffusions of each reactant that is a very difficult task. Hence, we assume two dominant mechanisms for oxygen and one for aluminum : prior to Al melting (933 K), gaseous oxygen released from CuO decomposition diffuses the most – which process is dominated by classical diffusion through the stable aluminum oxide based matrix, as demonstrated experimentally in[53]. Above Al melting, liquid aluminum starts diffusing through the porous and/or fractured materials that endures huge constraints upon melted Al. Then, as calculated from DFT calculations[55], we consider that O and Al react spontaneously when in contact. Hence, r_{Al2O3} characteristic time is much shorter compared to the ones of other physical mechanisms. Rigorously speaking, our model does not consider an instantaneous Al+O reaction but a reaction rate proportional to the inverse of the time step (see **Figure 1**). Nevertheless, it was assumed that the time step was small enough to consider this reaction as instantaneous. This means that oxygen presence decreases in Al rich regions due to Al-O reaction, limiting its spatial spreading.

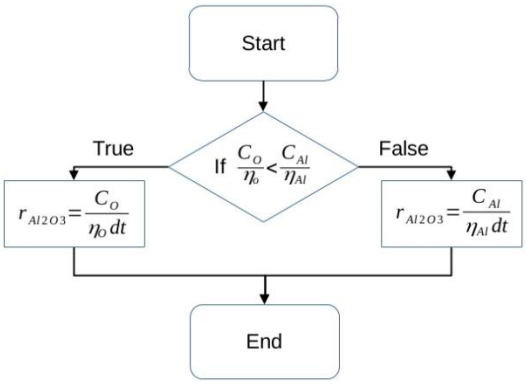

Figure 1. Details of the algorithm used to simulate the Al+O reaction rate, r_{Al2O3}, where η_o and η_{Al} are the stoichiometric coefficients of oxygen and aluminum, respectively.

Regarding the products, the alumina and copper diffusions are assumed to play a minor role in the combustion process. However, numerical convergence of the finite volume method imposes some minimal diffusivity of all species. We checked by running different simulations that those diffusions has a negligible impact on the combustion characteristics. Beyond the fact that huge discrepancies do exist in diffusion coefficient values in the literature [56-58], defining diffusion pathways and associated parameters for both Al and oxygen species of thermite steady state combustion is a vast issue, out of the reach of current understanding. Therefore, it is generally accepted to fit effective coefficients through specific set of measurements, whatever their nature [50, 59, 60]. We assume diffusion of species to follow a classical Arrhenius law as given in Equation 13 which defines how an Arrhenius law is implemented for species diffusion.

$$D_i|_{i=Al,O} = k_{0,i} e^{\frac{-Ea,i}{RT}} \tag{13}$$

where $k_{0,i}$ and $E_{a,i}$ represent the Arrhenius pre-exponent and activation energy, respectively for i (Al and O) species diffusion.

Finally, as it is impossible to quantify with accuracy the diffusion parameters of Al or oxygen, the diffusion of oxygen and aluminum are considered equal. The optimized parameters set for $k_0 = k_{0,O} = k_{0,Al}$ and $E_a = E_{a,O} = E_{a,Al}$ are 7.1×10^{-6} m^2/s and 73.6 kJ/mol, respectively. This optimized (E_a, k_0) set are fitted from a set of experimental results performed on different Al/CuO multilayers published in[48, 59] (See supplementary file S2). They are in the range of the usual published values for oxygen diffusion to treat propagation. For example, Brotman *et al.*[61] and Lahiner *et al.*[50] used k_0 = 1.16×10^{-6} m^2/s and E_a = 67.3 kJ/mol in the temperature range of 700 to 1030 K for atomic oxygen diffusion in copper/copper oxide, and k_0 = 9×10^{-5} m^2/s and E_a = 140 kJ/mol for atomic oxygen diffusion in alumina media based on the experimental data reported by Egan *et al.*[23]. The impact of diffusion values on propagation velocity is discussed in the Sec 4.3.

3.2. Boundary and initial conditions

The model system (see **Figure 2**) consists of *n*-Al/CuO bilayer burning without any loss in the environment. The bilayer thickness is defined as $t_b = t_{Al} + t_{CuO}$ with $t_{CuO} = \frac{1.9}{\varphi} \times t_{Al}$. φ is the equivalence ratio and t_{Al} and t_{CuO} are the Al and CuO thicknesses, respectively. Note that in a φ = 1 sample, the aluminum thickness is half the CuO thickness (stoichiometric stack) whereas φ > 1 corresponds to a fuel-rich situation with thicker aluminum layers.

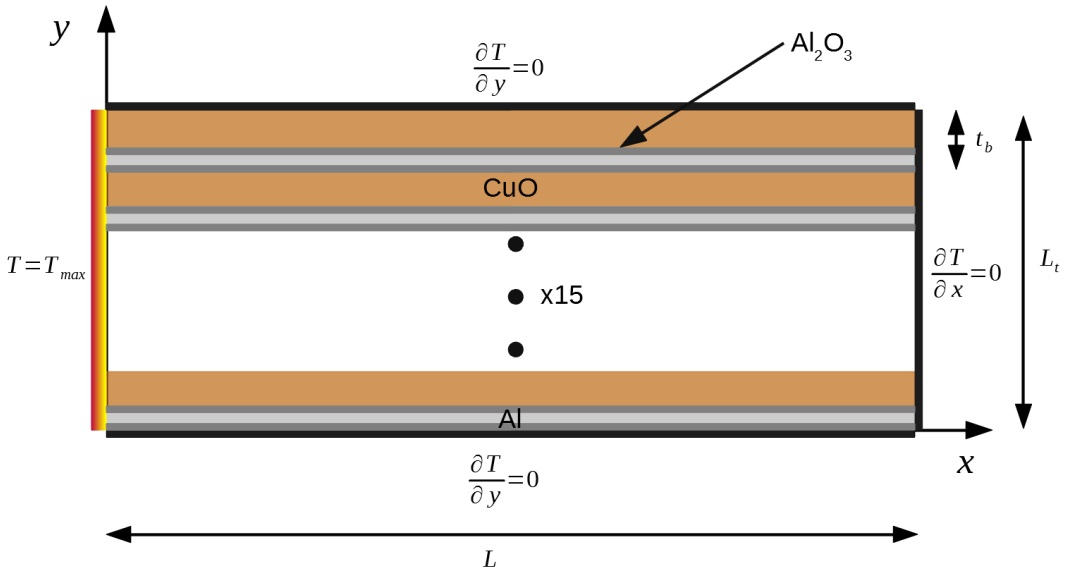

Figure 2. Schematic of the modeled Al/CuO multilayered system surrounded by a nonconductive media: the left end is burning and set to $T = T_{max}$, the reactive front temperature. Then, the reaction front propagates from the left to the right side of the film.

As initial conditions, the multilayer film is supposed to ignite at the left end, *i.e.* the temperature of the left boundary is set to a value T_{max} as discussed in the next paragraph. The rest of the multilayer is initially set at the ambient temperature. Finally, thermal losses through the boundaries are supposed to be null. Hence adiabatic conditions $\left(\frac{\partial T}{\partial y} = 0\right)$ are applied to both surfaces.

Over a certain unknown temperature, the additional effect of pressure and the phase change of the different species disintegrate the matter. All the disintegrated matter continues to react in the environment, but the generated heat is not transferred as efficiently as in the condensed state reaction. This results in an important heat flux decrease, which is considered in the model by limiting the temperature of the reaction (or flame temperature) numerically at a certain T_{max} value. Therefore, the heat fluxes, which are defined by a temperature gradient, are in turn limited. In the model, the temperature T_{max} is fixed to the adiabatic flame temperature of the Al/CuO reaction, 2843 K[62], also

corresponding to the copper vaporization point. The influence of T_{max} on the reaction front propagation velocity is theoretically evaluated and discussed in Sec. 4.2. Finally, as there is no mass exchange between the multilayer and the environment, the boundary conditions for all the species are defined as $\frac{\partial C_i}{\partial x} = \frac{\partial C_i}{\partial y} = 0$, where *i* stands for CuO, Al, Al_2O_3, Cu, and O.

4 Results

Here we consider the model system as described in **Figure 2**, *i.e.*, a thermite thin film composed of *n*-Al/CuO bilayers. A representative simulation output for Al/CuO multilayers reaction propagation is shown in **Figure 3**. In this image, the temperature field is represented by a heat map, where purple is cold (300 K) and yellow is hot (2843 K). Superimposed over the heat map are the y-average reaction profile of temperature, and y-average alumina concentration, which share the same x-axis but are scaled to fit on the detached (right) axis.

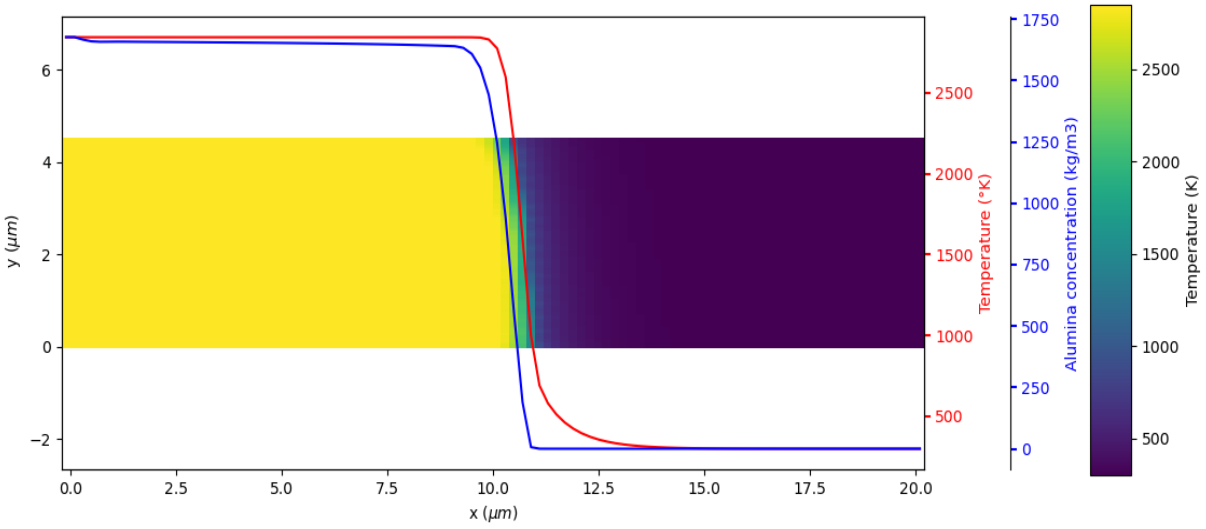

Figure 3. 2D simulation of a 4.5 μm thick Al/CuO multilayer. Temperature and alumina concentration are superimposed over the temperature field and scaled to fit on the detached (right)

axis; see legend for scale factors. The Al/CuO bilayer thickness is 300 nm and the equivalence ratio is 1. T_{max} is fixed at 2843 K.

Features of interest in these types of simulations include the steady reaction front propagation velocity, v, and the thermal profile of the reaction front. The width w_f of the reaction front is determined as the distance between the points where the temperature reaches 95% of the maximum temperature (T_{max}) and 105% of the minimum temperature (ambient).

4.1 Influence of multilayer parameters: film thickness, stoichiometry and bilayer thickness

We first investigate the influence of the equivalence ratio φ, on the reaction front propagation velocity, for a 4.5 μm thick Al/CuO multilayer. The results are presented in **Figure 4**. For $\varphi < 0.5$ the reaction quenches. As expected the reaction velocity increases with the equivalence ratio until it reaches a maximum value at 72 m/s. The propagation velocity obtained with an equivalence ratio of 7.4 is 44 m/s. A higher increase in the ratio quenches the reaction.

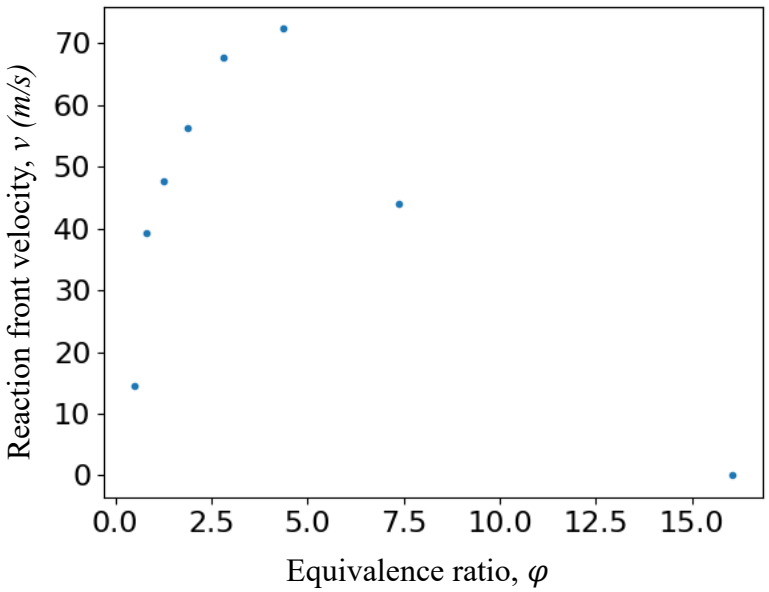

Figure 4. Simulation of the reaction front velocity of 4.5 μm thick Al/CuO multilayers as a function of the equivalence ratio, φ. The Al/CuO bilayer thickness is fixed at 300 nm, and T_{max} = 2843 K.

Next, we investigate the influence of the number of bilayers (3 to 21) and bilayer thickness (50 nm to 500 nm) on the reaction front propagation velocity, which are respectively shown in **Figure 5a** and **5b**, respectively. Note that in **Figure 5a**, the number of bilayers is fixed; in **Figure 5b**, the bilayer thickness is fixed. We observe a direct relationship between the reaction front velocity and the number of bilayers. For many bilayers (n > 20), the velocity tends toward 44 m/s. This is easily explained as for high number of bilayers, the average required mass transport distance for both oxygen and aluminum atoms is divided by two unlike the single layered system. This distance reduction decreases the reactive characteristic time and hence increases the front velocity.

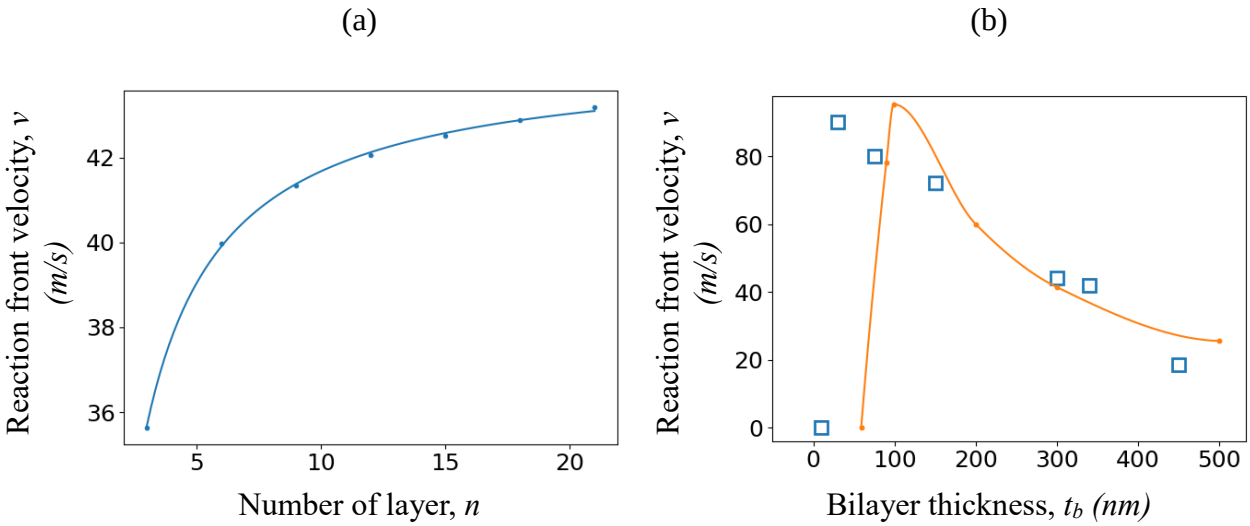

Figure 5. Simulation of front reaction velocity as a function of (a) number of bilayers, n (t_b = 300 nm), and (b) bilayer thickness, t_b (n = 15). The square markers correspond to experiments. For both curves, φ = 1, and T_{max} = 2843 K.

The effect of bilayer thickness on reaction front velocity shows the same global behavior as previously reported in several experimental works[39, 63]. We distinguish in **Figure 5b** the first regime for thick bilayers (t_b > 200 nm) with a propagation velocity decreasing slowly below 40 m/s. With the decrease in the bilayer thickness toward the nanoscale, the reaction velocity increases continuously up to a maximum (95 m/s) and then decreases sharply for ultrathin bilayers (t_b < 100 nm). Reducing t_b decreases the diffusion length and, consequently, increases the reaction front velocity. The

sharp drop observed for ultrathin bilayers results from the lack of sufficient chemical energy with respect to the total heat capacity of the Al_2O_3 interfacial films. The experiments (marked in **Figure 5b**) show good agreement with the simulation for t_b > 100 nm. For ultrathin bilayer, we can explain the increasing discrepancies between the simulation and experiment by the presence and increasing role of the natural interface, which is simulated as a 2 nm thick amorphous alumina, whereas it is an ill-defined mixture of Al, Cu, and O in real stacks.

4.2. Influence of heat fluxes lost in the environment due to film disintegration prior to combustion completion

As explained before, the reaction temperature was numerically limited to T_{max} to account for the disintegration of the reactant film before the completion of its combustion, which has been observed experimentally[41]. **Figure 6** shows that the average heat flux ($\varnothing_{av}$) along the combustion front, varies linearly with respect to T_{max}. Different observations can be further made (see **Figure 6a**): without constraining the maximal temperature $\varnothing_{av}$ = 420 GW/m², whereas when T_{max} = 1750 K, $\varnothing_{av}$ = 45 GW/m², which is almost a decade less. Therefore, limiting T_{max} to 1750 K is equivalent to considering an energy loss $\varnothing_{av.loss}$ of 370 GW/m², *i.e.* energy not provided to the energetic film to sustain the propagation. A rapid calculation show that limiting T_{max} to 1750 K is equivalent to consider that almost 90% of the reactants reacts in the air and is not used to sustain the front propagation.

Next, the influence of $\varnothing_{av.lost}$ on the reaction front velocity is investigated considering an Al/CuO film made of 15-300 nm thick Al/CuO stoichiometric bilayers. The results are presented in **Figure 6b.** The velocity varies linearly with respect to the flux. *v* is equal to 13 m/s for an average flux of 45 GW/m² and reaches a maximum of 91 m/s for 420 GW/m². The velocity is divided by almost a decade when the incoming heat flux is reduced by ten due to thermal loss in the environment. This result clearly demonstrates the great impact of the potential disintegration of the film prior to its

reaction completion on its combustion propagation. Ideally, this should be experimentally determined to obtain better quantitative prediction.

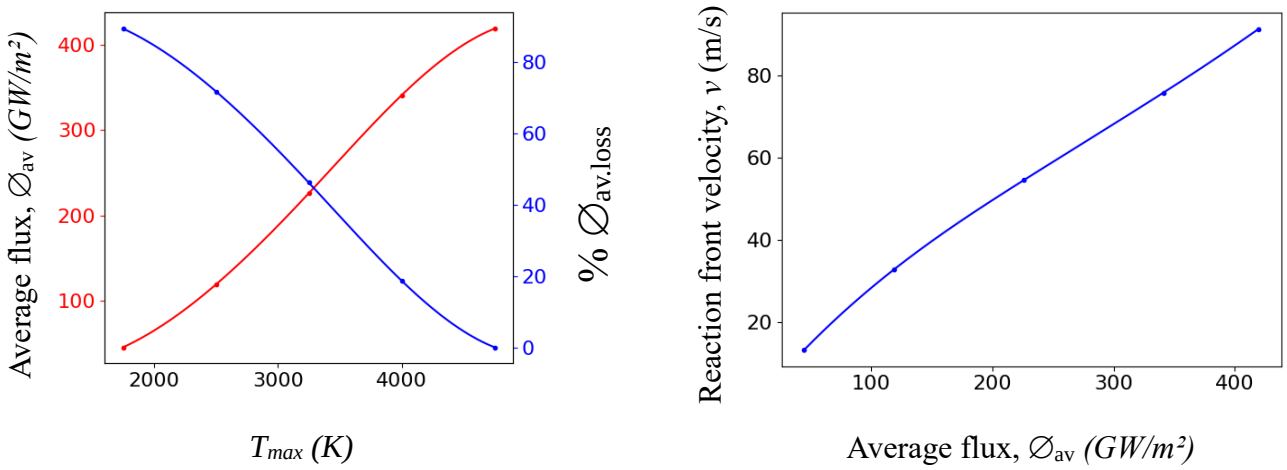

Figure 6. (a) Correlation between T_{max} and average heat flux (left y-scale) and percentage of heat flux lost in the environment (right y-scale). (b) Effect of average heat flux on reaction front velocity for a 4.5 µm thick stoichiometric stack. The Al/CuO bilayer thickness is fixed at 300 nm.

In summary, despite the unknowns on the redox chemistry side, the results demonstrated that the model is able to capture the velocity trends. The three main parameters that contribute to the uncertainty in the front propagation velocity prediction are the heat of reaction (supposed equal to theoretical ones[46] which is not the case), the thermal conductivity of species which varies with temperature, and T_{max}, which cannot be quantified rigorously due to the extreme difficulty in probing the multiphases reaction mechanisms. Other important uncertainties in the model come from the diffusion coefficients that may change drastically when modifying the deposition conditions, as they are controlled by the grain boundaries and mechanical stresses. One common method employed to estimate the E_a of systems featuring self-propagating combustion involves the dilution of the sample so that changes in combustion velocity are used to compute E_a. However, considering that this method

also inherently changes the chemistry of the reaction, it is not possible to apply it to our system. Therefore, the next section proposes to investigate the effect of varying the diffusion coefficient parameters k_0 and E_a, used to describe the diffusion of both Al and O species.

4.3 Impact of diffusion coefficients on the combustion properties

A parametric map of reaction velocity versus k_0 and E_a is plotted in **Figure 7**. k_0 and E_a range from 3.8×10^{-7} to 1.36×10^{-4} m²/s and from 20 kJ/mol to 170 kJ/mol, respectively. Note that in this mapping, we maintain the hypothesis that both O and Al diffuse equally.

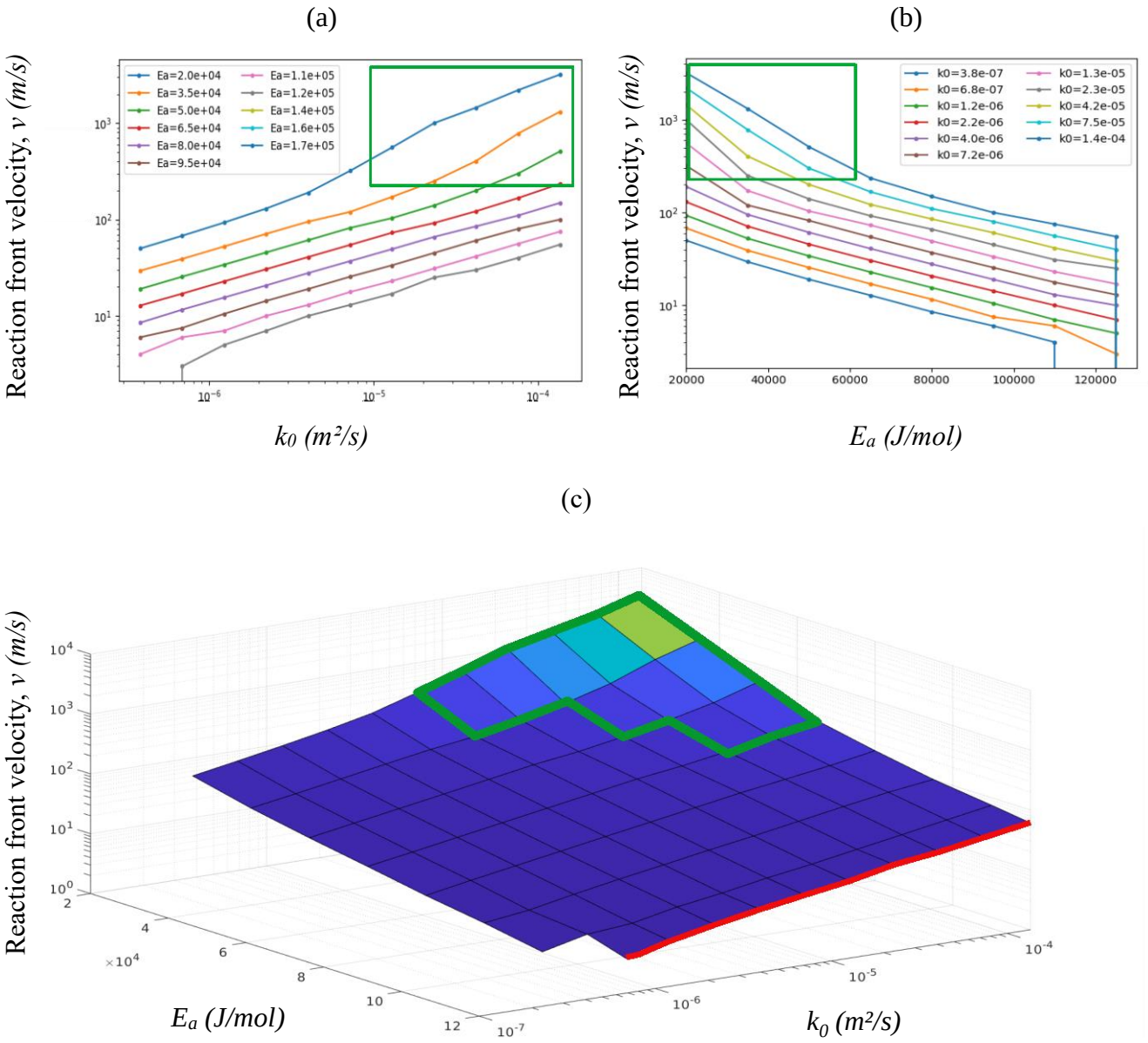

Figure 7. Velocity 2D map with respect to the activation energy *(E_a)* and prefactor *(k_0)* of the diffusion coefficient (a) velocity *vs.* prefactor, (b) velocity *vs.* activation energy E_a, (c) 2D map.

The whole combustion domain can be divided into three subdomains: inside the green outline, both oxygen and aluminum diffuse freely and at high speed, highly, greatly reducing the required time to travel and react. Consequently, the propagation is very fast and can reach hundreds and even thousands of m/s, which has never been observed experimentally. The temperature field and species

map show a highly corrugated front in the copper oxide material (see **Figure 8a**). This corrugation effect is provoked by a high concentration of oxygen accumulated in CuO, since its decomposition characteristic time becomes nonnegligible compared to the time of the diffusion of aluminum and oxygen species. Hence, in this region, the combustion process is controlled by the copper oxide decomposition rate. Despite the local corrugation of the reactive front, combustion is homogeneous and stable. Note that this combustion regime was never seen experimentally in Al/CuO thin films, where diffusion through alumina-based regions is a rate-limiting step for the reaction.

In the dark blue domain, *i.e.*, E_a < 125 kJ/mol, the form of the map shows that the front reaction velocity follows an exponential relationship with respect to the activation energy, E_a, and follows a power relation with respect to the prefactor, k_0. The front velocity ranges from ten m/s to one hundred m/s. The combustion regime is in the steady-state and front progression is constant and stable.

When E_a = 125 kJ/mol, the red frontier, the combustion occurs, but the reactive front velocity appears to be much slower and unstable. It is characterized by a series of oscillations (illustrated in **Figure 8b**) due to thermal instability that can lead to quenching of the reaction. These autooscillations have been reported in a variety of SHS systems and originate from the multistep reactions occurring in such systems, which have inherently different reaction rates[64-66].

For E_a > 125 kJ/mol, self-propagation is not possible.

(a)

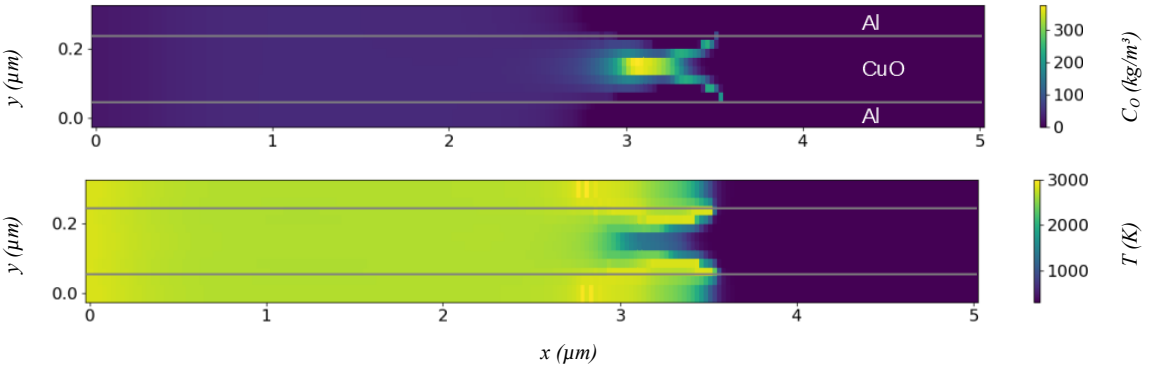

(b)

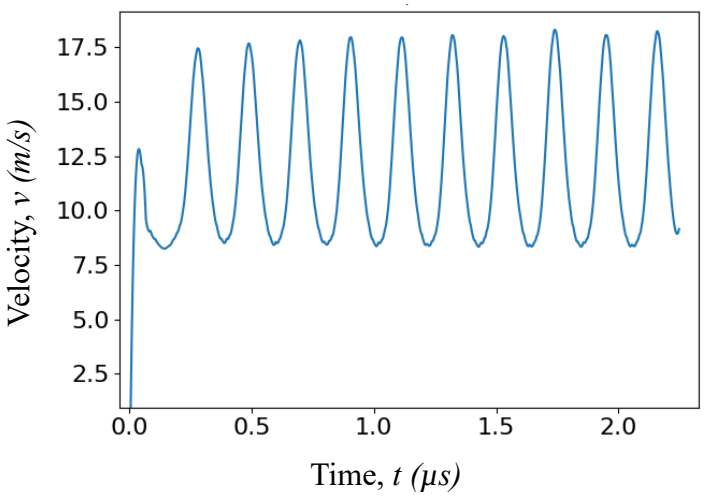

Figure 8. (a) Temperature and oxygen concentration 2D map for a 4.5 μm thick stoichiometric stack (t_b = 300 nm) simulated with $k_0 = 1.36\times10^{-4}$ m²/s and E_a = 20kJ/mol (v = 3100 m/s). (b) Reaction front velocity versus time for a 4.5 μm thick stoichiometric stack (t_b = 300 nm). Simulation performed with $k_0 = 7.18\times10^{-6}$ m²/s and E_a=125 kJ/mol.

From all data acquired through the simulated cases in **Figure 7**, we plot the evolution of the flame front width with the reaction front propagation velocity, differencing two different equivalence ratio (**Figure 9**). Different T_{max} values are also considered. Regardless of the condition of the simulation and stacks configuration, an inverse relationship between the reaction front velocity and the front width is found. w_f tends to a minimum value of 2 μm for high velocities (> 80 m/s) for both equivalence ratio. w_f is the maximum (8.5 μm) when the reaction front propagates at ~17 m/s (17.5 m/s for φ = 2 and 16 m/s for φ = 1).

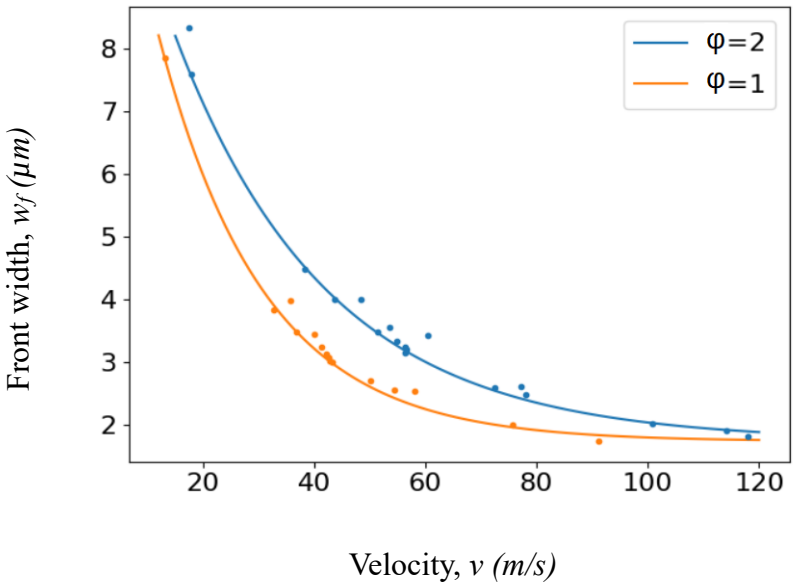

Figure 9. Relationship between front width and propagation velocity. Points correspond to simulations performed for different Al/CuO stacks as well as the same stacks with different T_{max} values and under different E_a and k_o conditions.

4.4 Inclusion of an inert metallic particle into the multilayer

Finally, to demonstrate the potential of this 2D model, we investigated the effect of adding one metallic particle (1.4 μm ×1 μm) into 15-300 nm thick bilayers (simulated length of 30 μm). Au was chosen, since it is chemically inert and features very high thermal diffusivity properties (127×10^{-6} m²/s) compared to CuO (9.90×10^{-6} m²/s) and Al (97×10^{-6} m²/s). Simulations were launched using the same initial and boundary conditions as simulations presented in Sec. 4.1. **Figure 10** presents temperature maps taken at three different times of simulation ($t_3 > t_2 > t_1$) to capture and map the reaction front crossing the Au particle.

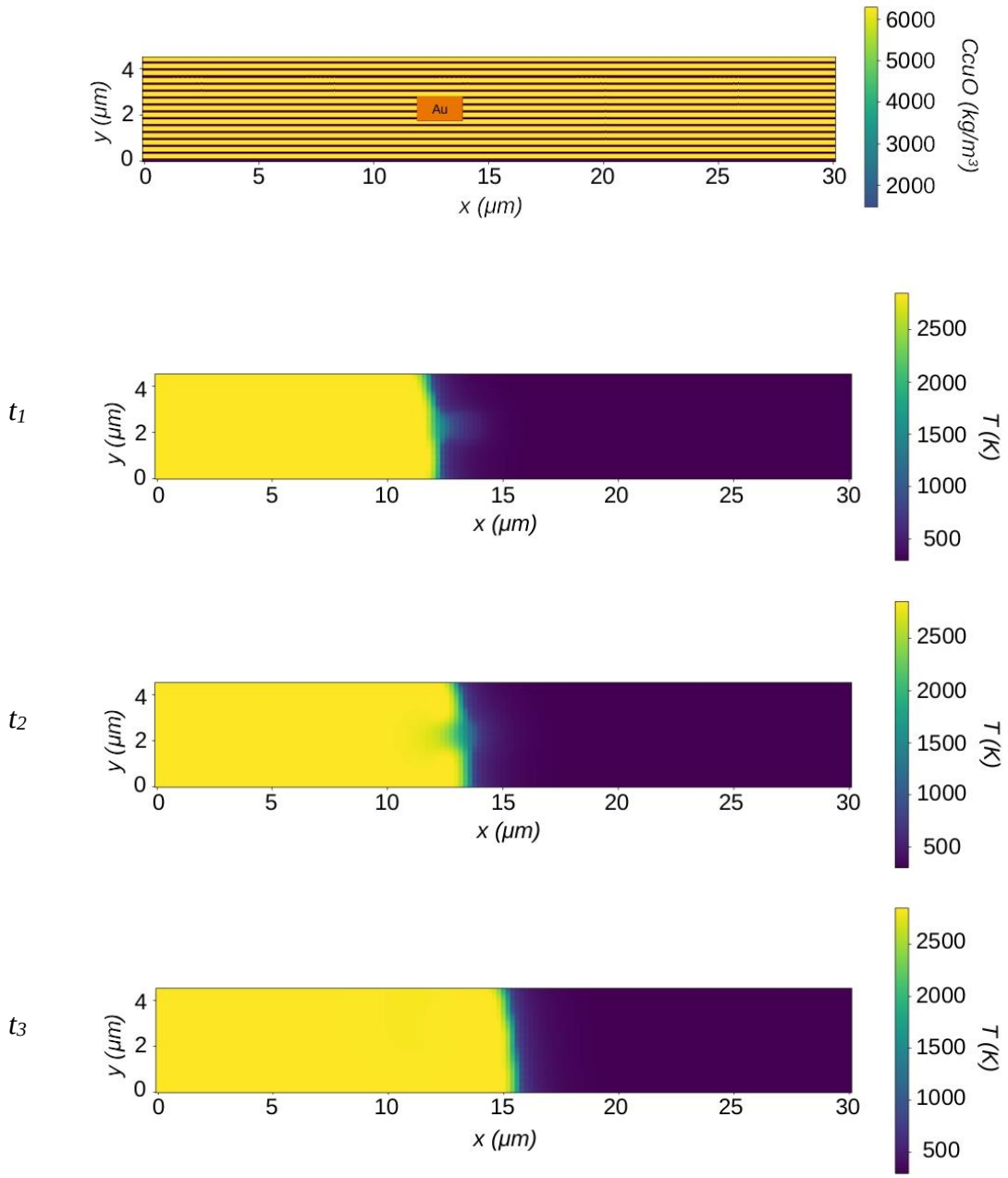

Figure 10. (top) Schematics of the modeled Al/CuO multilayered system in which a Au particle (1.4 μm ×1 μm) is included within the Al/CuO stack (4.5 μm in thickness by 30 μm in length). Yellow and blue colors correspond to CuO and Al, respectively. (bottom) 2D temperature maps showing the reaction front (light green thin zone) passing across the Au particle. The Al/CuO bilayer thickness is fixed at 300 nm, the equivalence ratio is 1, and T_{max} = 2843 K.

Approaching the inserted Au, the reaction front is distorted. First, the temperature field shows that the downstream Au becomes hotter than the adjacent zone: 850 K versus 500 K on the same y-axis (see **Figure 10**, t_1). This creates a hot spot that remains visible until the surrounding media starts reacting at t_2. Then, Au quickly becomes colder than the surroundings because it does not react. Finally, at t_3 the Au particle is thermalized at the same temperature as the rest of the multilayer. Corrugation of the front is illustrated by the plot of the y-average velocity versus time (**Figure 11**). We can distinguish 4 phases : ① a steady-state combustion regime of the reaction front prior to reaching the Au particle. ② an increase in the instantaneous velocity when the reaction front reaches the Au particle as gold conducts heat faster than thermite. ③ a drop in the instantaneous velocity when the front embodies the Au particle, because Au is also a good heat sink. And, ④ the steady-state combustion regime is re-established when the front has passed the Au particle. The average reaction front velocity is therefore a balance between the ability of the inserted particle to conduct heat (increasing the velocity) and absorb the heat produced by the reaction (decreasing the velocity).

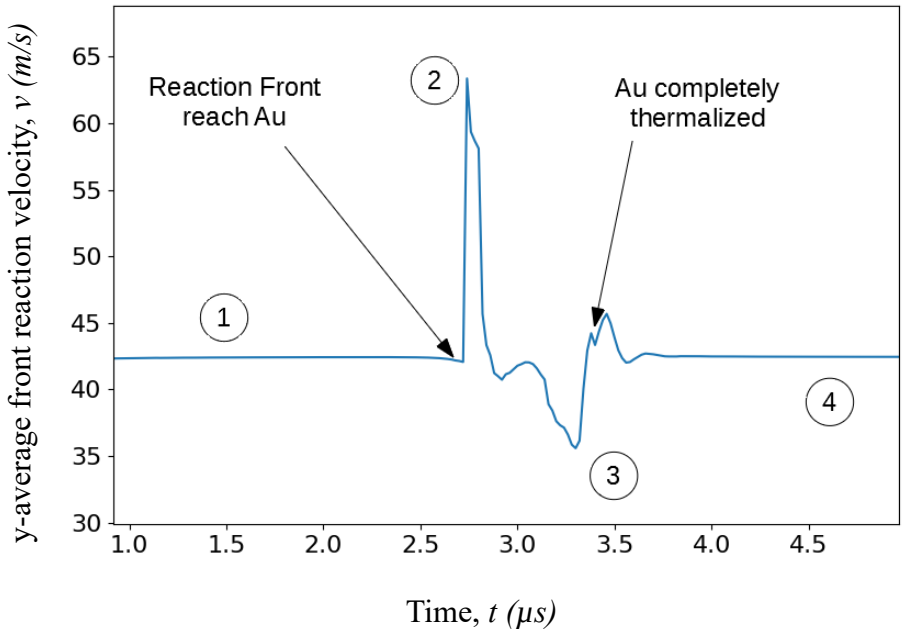

Figure 11. Y-average reaction front velocity versus time showing the four main combustion regimes when the reaction front approaches, goes through and passes the gold particle. The Al/CuO bilayer thickness is fixed at 300 nm, the equivalence ratio is 1 and T_{max} = 2843 K.

5 Conclusion

We developed a new 2D nonstationary model implementing both oxygen and Al diffusion and solving the differential equations for heat and mass transport and chemical reactions. The model was applied to the simulation of the combustion front propagation in free-standing Al/CuO multilayers. The model can be easily modified to account for any thermite structure, since the initial repartition, the reactants concentration as well as the thermite mixture can be chosen freely, as only a limited set of parameters is to be tuned. The model presented in this work not only predicts the reaction front progression rate dependency on multilayer dimensions and fuel concentration, but its 2D formulation allows for the prediction of how impurities affect reaction front progression. The simulations show that the presence of a metallic particle inside thermite provokes the microscopic corrugation of the reaction front. Indeed, the metal first boosts for the reaction velocity by helping the heat to propagate in the upfront region, and further slows down locally the front velocity. We discuss the nature of reaction propagation in an Al/CuO material that highly depends on the local heat transfer. In this

respect, we show the crucial role of film disintegration, which limits the maximum temperature that the film may reach. We also discuss the kinetic parameters governing mass transport during the reaction, *i.e.* diffusion coefficients: activation energies and prefactors. Under certain diffusion conditions the model exhibits unstable combustion (at E_a = 125 kJ/mol) and quenching (E_a > 125 kJ/mol). Additionally, simulations show that regardless of the Al/CuO configuration, the front width is an function of the reaction front velocity and is calculated to be between a couple of microns to 16 µm. Overall we believe that the 2D feature of our approach represents a great progress in the thermite reaction front dynamics modelling. Not only it allows investigating a diversity of 2D thermite structures, not only multilayers but also dense network of particles, but also, it opens the possibility to study the effect of inclusions (voids or other materials) on the flame front dynamics of the thermite.

Author information

Corresponding author

Corresponding to Dr. Carole Rossi, carole.rossi@laas.fr

Author contributions

E. Tichtchenko developed the model and performed calculations. A. Esteve and C. Rossi assisted E. Tichtchenko in the model implementation and results analysis. C. Rossi also provided support for manuscript preparation and supervised the research. The manuscript was written through contributions of all authors. All authors have given approval to the final version of the manuscript.

Competing financial interests

The authors declare no competing financial interests.

Funding Sources

C. Rossi received funding from the European Research Council (ERC) under the European Union's Horizon 2020 research and innovation programme (grant agreement No 832889 - PyroSafe).

Acknowledgment

The authors acknowledge support from the European Research Council (H2020 Excellent Science) Researcher Award (grant 832889 – PyroSafe).

4. References

[1] M.L. Pantoya, J.J. Granier, Combustion behavior of highly energetic thermites: Nano versus micron composites, Propell Explos Pyrot 30 (2005) 53-62.

[2] S. Apperson, R.V. Shende, S. Subramanian, D. Tappmeyer, S. Gangopadhyay, Z. Chen, K. Gangopadhyay, P. Redner, S. Nicholich, D. Kapoor, Generation of fast propagating combustion and shock waves with copper oxide/aluminum nanothermite composites, Appl Phys Lett 91 (2007).

[3] L. Glavier, G. Taton, J.M. Ducere, V. Baijot, S. Pinon, T. Calais, A. Esteve, M.D. Rouhani, C. Rossi, Nanoenergetics as pressure generator for nontoxic impact primers: Comparison of Al/Bi2O3, Al/CuO, Al/MoO3 nanothermites and Al/PTFE, Combust Flame 162 (2015) 1813-1820.

[4] K. Sullivan, M.R. Zachariah, Simultaneous Pressure and Optical Measurements of Nanoaluminum Thermites: Investigating the Reaction Mechanism, J Propul Power 26 (2010) 467-472.

[5] A.K. Stover, N.M. Krywopusk, J.D. Gibbins, T.P. Weihs, Mechanical fabrication of reactive metal laminate powders, J Mater Sci 49 (2014) 5821-5830.

[6] E.L. Dreizin, Metal-based reactive nanomaterials, Prog Energ Combust 35 (2009) 141-167.

[7] E.L. Dreizin, M. Schoenitz, M.A. Trunov, V.K. Hoffmann, S.M. Umbrajkar, E. Beloni, Reactive nanocomposite materials produced by arrested reactive milling, Theory and Practice of Energetic Materials, Vol Vii, (2007) 3-14.

[8] M. Mursalat, M. Schoenitz, E.L. Dreizin, Effect of premilling Al and CuO in acetonitrile on properties of Al center dot CuO thermites prepared by arrested reactive milling, Combust Flame 214 (2020) 57-64.

[9] S.H. Kim, M.R. Zachariah, Enhancing the rate of energy release from nanoenergetic materials by electrostatically enhanced assembly, Adv Mater 16 (2004) 1821-+.

[10] S. Palussiere, J. Cure, A. Nicollet, P. Fau, K. Fajerwerg, M.L. Kahn, A. Esteve, C. Rossi, The role of alkylamine in the stabilization of CuO nanoparticles as a determinant of the Al/CuO redox reaction, Phys Chem Chem Phys 21 (2019) 16180-16189.

[11] B.J. Clapsaddle, A.E. Gash, J.H. Satcher, R.L. Simpson, Silicon oxide in an iron(III) oxide matrix: the sol-gel synthesis and characterization of Fe-Si mixed oxide nanocomposites that contain iron oxide as the major phase, J Non-Cryst Solids 331 (2003) 190-201.

[12] F. Severac, P. Alphonse, A. Esteve, A. Bancaud, C. Rossi, High-Energy Al/CuO Nanocomposites Obtained by DNA-Directed Assembly, Adv Funct Mater 22 (2012) 323-329.

[13] T. Calais, D. Bourrier, A. Bancaud, Y. Chabal, A. Esteve, C. Rossi, DNA Grafting and Arrangement on Oxide Surfaces for Self-Assembly of Al and CuO Nanoparticles, Langmuir 33 (2017) 12193-12203.

[14] T. Calais, V. Baijot, M.D. Rouhani, D. Gauchard, Y.J. Chabal, C. Rossi, A. Esteve, General Strategy for the Design of DNA Coding Sequences Applied to Nanoparticle Assembly, Langmuir 32 (2016) 9676-9686.

[15] A.K. Murray, T. Isik, V. Ortalan, I.E. Gunduz, S.F. Son, G.T.C. Chiu, J.F. Rhoads, Two-component additive manufacturing of nanothermite structures via reactive inkjet printing, J Appl Phys 122 (2017).

[16] E.R. Wainwright, K.T. Sullivan, M.D. Grapes, Designer Direct Ink Write 3D-Printed Thermites with Tunable Energy Release Rates, Adv Eng Mater, (2019).

[17] Y.F. Mao, L. Zhong, X. Zhou, D.W. Zheng, X.Q. Zhang, T. Duan, F.D. Nie, B. Gao, D.J. Wang, 3D Printing of Micro-Architected Al/CuO-Based Nanothermite for Enhanced Combustion Performance, Adv Eng Mater 21 (2019).

[18] H.Y. Wang, J.P. Shen, D.J. Kline, N. Eckman, N.R. Agrawal, T. Wu, P. Wang, M.R. Zachariah, Direct Writing of a 90 wt% Particle Loading Nanothermite, Adv Mater 31 (2019).

[19] C. Rossi, Engineering of Al/CuO reactive multilayer thin films for tunable initiation and actuation, Propellants, Explosives, Pyrotechnics 44 (2019) 94-108.

[20] J.B. Xu, Y. Shen, C.G. Wang, J. Dai, Y. Tai, Y.H. Ye, R.Q. Shen, H.Y. Wang, M.R. Zachariah, Controlling the energetic characteristics of micro energy storage device by in situ deposition Al/MoO3 nanolaminates with varying internal structure, Chem Eng J 373 (2019) 345-354.

[21] A.H. Kinsey, R. Behrou, J.K. Guest, T.P. Weihs, Critical heat dissipation length scales in fully dense thermite foils, Combust Flame 190 (2018) 432-440.

[22] S. Fu, R.Q. Shen, P. Zhu, Y.H. Ye, Metal-interlayer-metal structured initiator containing Al/CuO reactive multilayer films that exhibits improved ignition properties, Sensor Actuat a-Phys 292 (2019) 198-204.

[23] G.C. Egan, E.J. Mily, J.P. Maria, M.R. Zachariah, Probing the Reaction Dynamics of Thermite Nanolaminates, J Phys Chem C 119 (2015) 20401-20408.

[24] G. Taton, D. Lagrange, V. Conedera, L. Renaud, C. Rossi, Micro-chip initiator realized by integrating Al/CuO multilayer nanothermite on polymeric membrane, J Micromech Microeng 23 (2013).

[25] L. Glavier, A. Nicollet, F. Jouot, B. Martin, J. Barberon, L. Renaud, C. Rossi, Nanothermite/RDX-Based Miniature Device for Impact Ignition of High Explosives, Propell Explos Pyrot 42 (2017) 307-316.

[26] X. Zhou, R.Q. Shen, Y.H. Ye, P. Zhu, Y. Hu, L.Z. Wu, Influence of Al/CuO reactive multilayer films additives on exploding foil initiator, J Appl Phys 110 (2011).

[27] A. Nicollet, G. Lahiner, A. Belisario, S. Souleille, M. Djafari-Rouhani, A. Esteve, C. Rossi, Investigation of Al/CuO multilayered thermite ignition, J Appl Phys 121 (2017).

[28] A. Nicollet, L. Salvagnac, V. Baijot, A. Estève, C. Rossi, Fast circuit breaker based on integration of Al/CuO nanothermites, Sensor Actuat a-Phys 273 (2018).

[29] H. Pezous, C. Rossi, M. Sanchez, F. Mathieu, X. Dollat, S. Charlot, V. Conedera, Fabrication, assembly and tests of a MEMS-based safe, arm and fire device, J Phys Chem Solids 71 (2010) 75-79.

[30] C. Rossi, B. Larangot, P.Q. Pham, D. Briand, N.F. de Rooij, M. Puig-Vidal, J. Samitier, Solid propellant microthrusters on silicon: Design, modeling, fabrication, and testing, J Microelectromech S 15 (2006) 1805-1815.

[31] G.A.A. Rodriguez, S. Suhard, C. Rossi, D. Esteve, P. Fau, S. Sabo-Etienne, A.F. Mingotaud, M. Mauzac, B. Chaudret, A microactuator based on the decomposition of an energetic material for disposable lab-on-chip applications: fabrication and test, J Micromech Microeng 19 (2009).

[32] B. Larangot, C. Rossi, T. Camps, A. Berthold, P. Pham, D. Briand, M. Puig-Vidal, P. Miribel, D. Esteve, N.D. Rooij, E. Montanes, G. Macias, J. Samitier, Solid Propellant Micro Rockets - Towards a New Type of Power MEMS in: AIAA (Ed.) NanoTech 2002 - "At the Edge of Revolution", Houston, Texas, 2002.

[33] J.P. Shen, Z.Q. Qiao, J. Wang, G.C. Yang, J. Chen, Z.Q. Li, X. Liao, H.Y. Wang, M.R. Zachariah, Reaction mechanism of Al-CuO nanothermites with addition of multilayer graphene, Thermochim Acta 666 (2018) 60-65.

[34] L. Marin, C.E. Nanayakkara, J.F. Veyan, B. Warot-Fonrose, S. Joulie, A. Esteve, C. Tenailleau, Y.J. Chabal, C. Rossi, Enhancing the Reactivity of Al/CuO Nanolaminates by Cu Incorporation at the Interfaces, Acs Appl Mater Inter 7 (2015) 11713-11718.

[35] L. Marin, Y.Z. Gao, M. Vallet, I. Abdallah, B. Warot-Fonrose, C. Tenailleau, A.T. Lucero, J. Kim, A. Esteve, Y.J. Chabal, C. Rossi, Performance Enhancement via Incorporation of ZnO Nanolayers in Energetic Al/CuO Multilayers, Langmuir 33 (2017) 11086-11093.

[36] K.T. Sullivan, W.A. Chiou, R. Fiore, M.R. Zachariah, In situ microscopy of rapidly heated nano-Al and nano-Al/WO3 thermites, Appl Phys Lett 97 (2010).

[37] S.M. Umbrajkar, M. Schoenitz, E.L. Dreizin, Exothermic reactions in Al-CuO nanocomposites, Thermochim Acta 451 (2006) 34-43.

[38] A.H. Kinsey, K. Slusarski, K. Woll, D. Gibbins, T.P. Weihs, Effect of dilution on reaction properties and bonds formed using mechanically processed dilute thermite foils, J Mater Sci 51 (2016) 5738-5749.

[39] M. Bahrami, G. Taton, V. Conedera, L. Salvagnac, C. Tenailleau, P. Alphonse, C. Rossi, Magnetron Sputtered Al-CuO Nanolaminates: Effect of Stoichiometry and Layers Thickness on Energy Release and Burning Rate, Propell Explos Pyrot 39 (2014) 365-373.

[40] K.J. Blobaum, A.J. Wagner, J.M. Plitzko, D. Van Heerden, D.H. Fairbrother, T.P. Weihs, Investigating the reaction path and growth kinetics in CuOx/Al multilayer foils, J Appl Phys 94 (2003) 2923-2929.

[41] J. Zapata, A. Nicollet, B. Julien, G. Lahiner, A. Esteve, C. Rossi, Self-propagating combustion of sputter-deposited Al/CuO nanolaminates, Combust Flame 205 (2019) 389-396.

[42] V. Turlo, O. Politano, F. Baras, Alloying propagation in nanometric Ni/Al multilayers: A molecular dynamics study, J Appl Phys 121 (2017).

[43] V. Turlo, O. Politano, F. Baras, Modeling self-sustaining waves of exothermic dissolution in nanometric Ni-Al multilayers, Acta Mater 120 (2016) 189-204.

[44] J.P. Zhang, Y.Y. Zhang, H. Li, J.X. Gao, X.L. Cheng, Molecular dynamics investigation of thermite reaction behavior of nanostructured Al/SiO2 system, Acta Phys Sin-Ch Ed 63 (2014).

[45] H.D. Zeng, Z.Y. Zhu, J.D. Zhang, X.L. Cheng, Diffusion and thermite reaction process of film-honeycomb Al/NiO nanothermite: Molecular dynamics simulations using ReaxFF reactive force field, Chinese Phys B 26 (2017).

[46] F. Shimojo, A. Nakano, R.K. Kalia, P. Vashishta, Enhanced reactivity of nanoenergetic materials: A first-principles molecular dynamics study based on divide-and-conquer density functional theory, Appl Phys Lett 95 (2009).

[47] G.L. Xiong, C.H. Yang, W.H. Zhu, Interface reaction processes and reactive properties of Al/CuO nanothermite: An ab initio molecular dynamics simulation, Appl Surf Sci 459 (2018) 835-844.

[48] H.Y. Wang, B. Julien, D.J. Kline, Z. Alibay, M.C. Rehwoldt, C. Rossi, M.R. Zachariah, Probing the Reaction Zone of Nanolaminates at similar to mu s Time and similar to mu m Spatial Resolution, J Phys Chem C 124 (2020) 13679-13687.

[49] K.M. Armstrong R, Combustion & plasma synthesis of high temperature materials., in: N.Y. VCH (Ed.), New york, 1990, pp. 88.

[50] G. Lahiner, A. Nicollet, J. Zapata, L. Marín, N. Richard, M. Djafari-Rouhani, C. Rossi, A. Estève, A diffusion–reaction scheme for modeling ignition and self-propagating reactions in Al/CuO multilayered thin films J Appl Phys 122 (2017).

[51] N. Amini-Manesh, S. Basu, R. Kumar, Modeling of a reacting nanofilm on a composite substrate, Energy 36 (2011) 1688-1697.

[52] M.V. Coulet, B. Rufino, P.H. Esposito, T. Neisius, O. Isnard, R. Denoyel, Oxidation Mechanism of Aluminum Nanopowders, J Phys Chem C 119 (2015) 25063-25070.

[53] I. Abdallah, J. Zapata, G. Lahiner, B. Warot-Fonrose, J. Cure, Y. Chabal, A. Esteve, C. Rossi, Structure and Chemical Characterization at the Atomic Level of Reactions in Al/CuO Multilayers, ACS Applied Energy Materials 1 (2018) 17-62.

[54] D. Stamatis, A. Ermoline, E.L. Dreizin, A multi-step reaction model for ignition of fully-dense Al-CuO nanocomposite powders, Combust Theor Model 16 (2012) 1011-1028.

[55] C. Lanthony, J.M. Ducere, M.D. Rouhani, A. Hemeryck, A. Esteve, C. Rossi, On the early stage of aluminum oxidation: An extraction mechanism via oxygen cooperation, J Chem Phys 137 (2012).

[56] A.E. Paladino, W.D. Kingery, Aluminum Ion Diffusion in Aluminum Oxide The Journal of Chemical Physics 37 (1962) 957-962.

[57] M. Garcia-Mendez, N. Valles-Villarreal, G.A. Hirata-Flores, M.H. Farias, Study of thermal diffusion between Al2O3 and Al thin films, Appl Surf Sci 151 (1999) 139-147.

[58] T. Campbell, R.K. Kalia, A. Nakano, P. Vashishta, S. Ogata, S. Rodgers, Dynamics of oxidation of aluminum nanoclusters using variable charge molecular-dynamics simulations on parallel computers, Phys Rev Lett 82 (1999) 4866-4869.

[59] A. Esteve, G. Lahiner, B. Julien, S. Vivies, N. Richard, C. Rossi, How Thermal Aging Affects Ignition and Combustion Properties of Reactive Al/CuO Nanolaminates: A Joint Theoretical/Experimental Study, Nanomaterials (Basel) 10 (2020).

[60] V. Baijot, D.R. Mehdi, C. Rossi, A. Esteve, A multi-phase micro-kinetic model for simulating aluminum based thermite reactions, Combust Flame 180 (2017) 10-19.

[61] S. Brotman, M.D. Rouhani, C. Rossi, A. Esteve, A condensed phase model of the initial Al/CuO reaction stage to interpret experimental findings, J Appl Phys 125 (2019).

[62] M.G. S. Fischer, A survey of combustible metals, thermites, and intermetallics for pyrotechnic applications, in: American Institute of Aeronautics and Astronautics, doi:doi:10.2514/6.1996-3018.(1996).

[63] N.A. Manesh, S. Basu, R. Kumar, Experimental flame speed in multi-layered nano-energetic materials, Combust Flame 157 (2010) 476-480.

[64] T.L. Jackson, J. Buckmaster, Heterogeneous propellant combustion, Aiaa J 40 (2002) 1122-1130.

[65] M. Chen, J. Buckmaster, T.L. Jackson, L. Massa, Homogenization issues and the combustion of heterogeneous solid propellants, P Combust Inst 29 (2002) 2923-2929.

[66] J.Y. Zhang, Z.Y. Fu, W.M. Wang, Q.J. Zhang, Theoretical study on auto-oscillating combustion in self-propagating high temperature synthesis, J Wuhan Univ Technol 18 (2003) 32-34.